An 800 million solar mass black hole in a significantly neutral universe at redshift 7.5

Eduardo Bañados[1,*], Bram P. Venemans[2], Chiara Mazzucchelli[2], Emanuele P. Farina[2], Fabian Walter[2], Feige Wang[3,4], Roberto Decarli[2,5], Daniel Stern[6], Xiaohui Fan[7], Fred Davies[8], Joseph F. Hennawi[8], Rob Simcoe[9], Monica L. Turner[9,10], Hans-Walter Rix[2], Jinyi Yang[3,4], Daniel D. Kelson[1], Gwen Rudie[1], and Jan Martin Winters[11]

[1]The Observatories of the Carnegie Institution for Science, 813 Santa Barbara St., Pasadena, CA 91101, USA
[2]Max Planck Institut für Astronomie, Königstuhl 17, D-69117, Heidelberg, Germany
[3]Department of Astronomy, School of Physics, Peking University, Beijing 100871, China
[4]Kavli Institute for Astronomy and Astrophysics, Peking University, Beijing 100871, China
[5]INAF – Osservatorio Astronomico di Bologna, via Gobetti 93/3, 40129, Bologna, Italy
[6]Jet Propulsion Laboratory, California Institute of Technology, 4800 Oak Grove Drive, Pasadena, CA 91109, USA
[7]Steward Observatory, The University of Arizona, 933 North Cherry Avenue, Tucson, AZ 85721–0065, USA
[8]Department of Physics, Broida Hall, University of California, Santa Barbara, CA 93106–9530, USA
[9]MIT-Kavli Center for Astrophysics and Space Research, 77 Massachusetts Avenue, Cambridge, MA, 02139, USA
[10]Las Cumbres Observatory, 6740 Cortona Dr, Goleta, CA 93117, USA
[11]Institut de Radioastronomie Millimétrique (IRAM), 300 rue de la Piscine, 38406 Saint Martin d'Hères, France
[*]ebanados@carnegiescience.edu

arXiv:1712.01860v1 [astro-ph.GA] 5 Dec 2017

ABSTRACT

Quasars are the most luminous non-transient objects known, and as such, they enable unparalleled studies of the universe at the earliest cosmic epochs. However, despite extensive efforts from the astronomical community, the quasar ULAS J1120+0641 at $z = 7.09$ (hereafter J1120+0641) has remained as the only one known at $z > 7$ for more than half a decade[1]. Here we report observations of the quasar ULAS J134208.10+092838.61 (hereafter J1342+0928) at a redshift of $z = 7.54$. This quasar has a bolometric luminosity of $4 \times 10^{13}\,L_\odot$ and a black hole mass of $8 \times 10^8\,M_\odot$. The existence of this supermassive black hole when the universe was only 690 Myr old, i.e., just 5% its current age, reinforces early black hole growth models that allow black holes with initial masses $\gtrsim 10^4\,M_\odot$[2,3] or episodic hyper-Eddington accretion[4,5]. We see strong evidence of the quasar's Lyα emission line being absorbed by a Gunn-Peterson damping wing from the intergalactic medium, as would be expected if the intergalactic hydrogen surrounding J1342+0928 is significantly neutral. We derive a significant neutral fraction, although the exact value depends on the modeling. However, even in our most conservative analysis we find $\bar{x}_{\rm HI} > 0.33$ ($\bar{x}_{\rm HI} > 0.11$) at 68% (95%) probability, indicating that we are probing well within the reionization epoch.

We selected the quasar J1342 + 0928 as part of an on-going effort to find $z > 7$ quasars by mining three large area surveys: the *Wide-field Infrared Survey Explorer*[6] (ALLWISE), the United Kingdom Infrared Telescope Infrared Deep Sky Survey (UKIDSS) Large Area Survey[7], and the DECam Legacy Survey (DECaLS; http://legacysurvey.org/decamls). At redshift $z \gtrsim 7$, residual neutral hydrogen in the intergalactic medium (IGM) absorbs virtually all flux blueward of the Lyα emission line, redshifted to observed wavelengths of $\gtrsim 1\,\mu$m, making quasars drop out of the optical bands entirely. We therefore required a detection in both UKIDSS J and *WISE* $W1$ bands with a signal-to-noise ratio (S/N) greater than 5 and no source in the DECaLS DR3 catalog within $3''$. We then performed forced photometry in the

DECaLS $z_{\rm DE}$-band image to confirm the non-detection, requiring a drop in flux of $z_{\rm DE,3\sigma} - J > 2$. We also required a flat spectral energy distribution to remove a large fraction of the most common contaminants of $z \gtrsim 7$ quasar searches[8]: low-mass brown dwarfs in our Galaxy. The survey photometry used to identify J1342+0928 is listed in Extended Data Table 1.

We confirmed J1342+0928 as a quasar with a 10 min spectrum with the Folded-port InfraRed Echellette (FIRE) spectrograph in the prism mode at the Magellan 6.5 m Baade telescope at Las Campanas Observatory on 09 March 2017. To analyze the emission line properties in greater detail, we obtained deeper and higher resolution spectra with FIRE, the LBT Utility Camera in the Infrared (LUCI) spectrograph at the Large Binocular Telescope, and the Gemini Near-Infrared Spectrograph (GNIRS) at the Gemini North telescope. The LUCI spectrum provided the first detection of the Mg II emission line at $\sim$2.4 μm but it was superseded by the higher S/N and larger wavelength coverage of the GNIRS spectrum. We also obtained deep follow-up photometry with the Magellan/Fourstar infrared camera on 19 March 2017. These data were used to bring the spectra to an absolute flux scale, compensating for slit-losses. The combined spectrum and follow-up photometry of J1342+0928 are shown in Figure 1.

The systemic redshift of this quasar is $z = 7.5413 \pm 0.0007$, measured through IRAM NOEMA observations of the [C II] 158 μm emission line from its host galaxy[9]. The redshift measured from a Gaussian fit to the Mg II line (see Figure 1) is 7.527 ± 0.004, i.e., blueshifted by $500 \pm 140\,{\rm km\,s^{-1}}$ with respect to the systemic redshift. This is consistent with the velocity offsets observed in other $z > 6$ quasars[10]. Adopting a cosmology[11] with $H_0 = 67.7\,{\rm km\,s^{-1}\,Mpc^{-1}}$, $\Omega_M = 0.307$, and $\Omega_\Lambda = 0.693$, this quasar is situated at a cosmic age of just 690 Myr after the Big Bang, i.e., when the universe was $\sim$10% younger than at the redshift of the previous most distant quasar known[1], at times when conditions in the universe were changing rapidly[12].

The mass of the quasar's central black hole can be estimated through the quasar luminosity and the full-width at half maximum (FWHM) of its Mg II line, under the assumption that local scaling relations[13] are still valid at high luminosity and high redshift[14]. The apparent ultraviolet magnitude measured at rest-frame 1450 Å from the quasar spectrum is $m_{1450} = 20.34 \pm 0.04$, which translates to an absolute magnitude of $M_{1450} = -26.76 \pm 0.04$. To calculate the quasar bolometric luminosity ($L_{\rm Bol}$), we first fit a power-law continuum to the spectrum and measure the luminosity at rest-frame 3000 Å (L_{3000}). We then use the bolometric correction[15] $L_{\rm Bol} = 5.15 \times L_{3000}$, resulting in $L_{\rm Bol} = 4.0 \times 10^{13}\,L_\odot$. The Mg II line has a FWHM of $2500^{+480}_{-320}\,{\rm km\,s^{-1}}$ (see inset in Figure 1), which together with the luminosity yields a black hole mass of $7.8^{+3.3}_{-1.9} \times 10^8\,M_\odot$. The reported errors do not include the dominant systematic uncertainties in the local scaling relations[13] of 0.55 dex. The accretion rate of this quasar is consistent with Eddington accretion, with an Eddington ratio of $L_{\rm Bol}/L_{\rm Edd} = 1.5^{+0.5}_{-0.4}$.

The existence of supermassive black holes in the early universe poses crucial questions on their formation and growth processes. Observationally, the most distant quasars provide joint constraints on black hole mass seed and accretion efficiency. Assuming a typical matter-energy conversion efficiency[4] of 10%, a black hole accreting at the Eddington rate grows exponentially on timescales of $\sim$50 Myr. Figure 2 shows the black hole growth of three quasars assuming that they accrete at the Eddington limit during their entire life. These are the quasars that currently place the strongest constraints on early black hole growth: J1342+0928 at $z = 7.54$, J1120+0641 at $z = 7.09$[1], and SDSS J0100+2802 at $z = 6.33$[16]. In all three cases, black hole seeds of at least $1000\,M_\odot$ are required by $z = 40$. The existence of these supermassive black holes at $z > 7$ is at odds with early black hole formation models that do not involve either massive ($\gtrsim 10^4\,M_\odot$) seeds or episodes of hyper-Eddington accretion.

The epoch of reionization was the universe's last major phase transition, when it changed from being completely neutral to ionized. The presence of complete Gunn-Peterson troughs in the spectra of $z \gtrsim 6$

quasars indicates that there were only traces of neutral hydrogen ($\bar{x}_{\rm HI} \sim 10^{-4}$) at $z \sim 6$. Because the Lyα transition saturates at larger neutral fraction, Gunn-Peterson troughs are only sensitive to the end phases of reionization[17]. Therefore, to probe the epoch when reionization occurred, we need alternative methods. During earlier stages of reionization ($\bar{x}_{\rm HI} > 0.1$), neutral intergalactic matter should produce characteristic damped Gunn-Peterson absorption *redward* of the Lyα emission line[18]. Evidence of this long-sought signature in quasar spectra has only been reported once, in the previous redshift-record holder at $z = 7.09$[1,19,20].

To calculate the implied IGM neutral fraction $\bar{x}_{\rm HI}$, one must first estimate the shape of the unabsorbed continuum, and then fit a parameterized absorption model using the data and continuum as inputs. This analysis is challenging because assumptions about the process of reionization need to be made and estimating the intrinsic strength of the Lyα emission for one single quasar is not straightforward. The latter is particularly difficult for the case of J1342+0928, which has extreme line blueshifts, which greatly reduces the number of lower-redshift quasars with which this source can be compared. In Figure 3 we summarize our approach, where we have followed previous works[1,20] to estimate the intrinsic continuum by searching for lower redshift quasars with similar spectral features and obtained an estimate of the neutral fraction following the method outlined by Miralda-Escudé (1998)[18]. The main result is that a significantly neutral IGM is required to reproduce the Lyα damping wing profile of J1342+0928. We find $\bar{x}_{\rm HI} = 0.55^{+0.22}_{-0.17}$, with the 95% central interval of the $\bar{x}_{\rm HI}$ distribution being between 0.26 and 0.93 (see Figure 3). To explore how robust this result is, we introduce an alternative quasar intrinsic emission model and two more elaborated methods to model the IGM damping wing in the Methods section. All our analyses strongly favour a scenario where the IGM surrounding J1342+0928 is significantly neutral although the exact value depends on the method (see Extended Data Table 2). Nevertheless, even our most conservative case indicates $\bar{x}_{\rm HI} > 0.11$ at 95% probability. We emphasize that higher S/N and larger wavelength coverage of the quasar's spectrum would be critical to refine and strengthen this result.

An important caveat is that a similar absorption profile could also be caused by a single high column density absorber ($N_{\rm HI} > 2 \times 10^{20}\,{\rm cm}^{-2}$) in the immediate vicinity of the quasar[18]. Although we find a large number of foreground heavy-element absorbers at lower redshifts, we find no evidence for metal-line absorption at redshifts near that of the quasar. Adopting the methodology of Simcoe et al. (2012)[21], a single Lyα absorber at $z = 7.49 \pm 0.01$ and $N_{\rm HI} = 10^{20.50^{+0.32}_{-0.45}}\,{\rm cm}^{-2}$ could produce the damping wing observed in J1342+0928. However, this absorber could have at most a metal abundance of $1/1700$ the Solar value for oxygen (95% confidence), which would make it among the most distant and metal-poor absorbers known[21]. The probability of intercepting a discrete absorber with $N_{\rm HI} \gtrsim 10^{20.5}\,{\rm cm}^{-2}$ within $2000\,{\rm km\,s}^{-1}$ of a quasar at $z = 7.5$ is less than 1%, based on the number density of such systems at lower redshifts[22]. This low probability supports the hypothesis that the absorption profile in J1342+0928 is instead probing the neutral IGM gas in the epoch of reionization.

Finally, the fact that both quasars known at $z > 7$ present evidence of Lyα damping wings confirms that we are starting to probe well within the epoch of reionization (see Figure 4), in agreement with recent indications based on the number density of Lyα emitting galaxies at similar redshifts[23] and results from the Cosmic Microwave Background[12].

References

1. Mortlock, D. J. *et al.* A luminous quasar at a redshift of z = 7.085. *Nat.* **474**, 616–619 (2011). DOI 10.1038/nature10159. 1106.6088.

2. Latif, M. A., Schleicher, D. R. G., Schmidt, W. & Niemeyer, J. Black hole formation in the early Universe. *Mon. Not. R. Astron. Soc.* **433**, 1607–1618 (2013). DOI 10.1093/mnras/stt834.

1304.0962.

3. Alexander, T. & Natarajan, P. Rapid growth of seed black holes in the early universe by supra-exponential accretion. *Sci.* **345**, 1330–1333 (2014). DOI 10.1126/science.1251053. 1408.1718.

4. Pacucci, F., Volonteri, M. & Ferrara, A. The growth efficiency of high-redshift black holes. *Mon. Not. R. Astron. Soc.* **452**, 1922–1933 (2015). DOI 10.1093/mnras/stv1465. 1506.04750.

5. Inayoshi, K., Haiman, Z. & Ostriker, J. P. Hyper-Eddington accretion flows on to massive black holes. *Mon. Not. R. Astron. Soc.* **459**, 3738–3755 (2016). DOI 10.1093/mnras/stw836. 1511.02116.

6. Wright, E. L. *et al.* The Wide-field Infrared Survey Explorer (WISE): Mission Description and Initial On-orbit Performance. *Astron. J.* **140**, 1868–1881 (2010). DOI 10.1088/0004-6256/140/6/1868. 1008.0031.

7. Lawrence, A. *et al.* The UKIRT Infrared Deep Sky Survey (UKIDSS). *Mon. Not. R. Astron. Soc.* **379**, 1599–1617 (2007). DOI 10.1111/j.1365-2966.2007.12040.x. arXiv:astro-ph/0604426.

8. Bañados, E. *et al.* The Pan-STARRS1 Distant z $>$ 5.6 Quasar Survey: More than 100 Quasars within the First Gyr of the Universe. *Astrophys. J. Suppl. Ser.* **227**, 11 (2016). DOI 10.3847/0067-0049/227/1/11. 1608.03279.

9. Venemans, B. P. *et al.* Copious amounts of dust and gas in a $z = 7.5$ quasar host galaxy. *Astrophys. J* Letters (2017). DOI 10.3847/2041-8213/aa943a.

10. Venemans, B. P. *et al.* Bright [C ii] and Dust Emission in Three z $>$ 6.6 Quasar Host Galaxies Observed by ALMA. *Astrophys. J* **816**, 37 (2016). DOI 10.3847/0004-637X/816/1/37. 1511.07432.

11. Planck Collaboration *et al.* Planck 2015 results. XIII. Cosmological parameters. *Astron. Astrophys.* **594**, A13 (2016). DOI 10.1051/0004-6361/201525830. 1502.01589.

12. Planck Collaboration *et al.* Planck intermediate results. XLVII. Planck constraints on reionization history. *Astron. Astrophys.* **596**, A108 (2016). DOI 10.1051/0004-6361/201628897. 1605.03507.

13. Vestergaard, M. & Osmer, P. S. Mass Functions of the Active Black Holes in Distant Quasars from the Large Bright Quasar Survey, the Bright Quasar Survey, and the Color-selected Sample of the SDSS Fall Equatorial Stripe. *Astrophys. J* **699**, 800–816 (2009). DOI 10.1088/0004-637X/699/1/800. 0904.3348.

14. Mejía-Restrepo, J. E., Lira, P., Netzer, H., Trakhtenbrot, B. & Capellupo, D. M. The effect of nuclear gas distribution on the mass determination of supermassive black holes. *Nat. Astron.* (2017). DOI 10.1038/s41550-017-0305-z. 1709.05345.

15. Richards, G. T. *et al.* Spectral Energy Distributions and Multiwavelength Selection of Type 1 Quasars. *Astrophys. J. Suppl. Ser.* **166**, 470–497 (2006). DOI 10.1086/506525. arXiv:astro-ph/0601558.

16. Wu, X.-B. *et al.* An ultraluminous quasar with a twelve-billion-solar-mass black hole at redshift 6.30. *Nat.* **518**, 512–515 (2015). DOI 10.1038/nature14241. 1502.07418.

17. Becker, G. D. *et al.* Evidence of patchy hydrogen reionization from an extreme Lyα trough below redshift six. *Mon. Not. R. Astron. Soc.* **447**, 3402–3419 (2015). DOI 10.1093/mnras/stu2646. 1407.4850.

18. Miralda-Escudé, J. Reionization of the Intergalactic Medium and the Damping Wing of the Gunn-Peterson Trough. *Astrophys. J* **501**, 15–22 (1998). DOI 10.1086/305799. astro-ph/9708253.

19. Greig, B., Mesinger, A., Haiman, Z. & Simcoe, R. A. Are we witnessing the epoch of reionisation at z = 7.1 from the spectrum of J1120+0641? *Mon. Not. R. Astron. Soc.* (2016). DOI 10.1093/mnras/stw3351. 1606.00441.

20. Bosman, S. E. I. & Becker, G. D. Re-examining the case for neutral gas near the redshift 7 quasar ULAS J1120+0641. *Mon. Not. R. Astron. Soc.* **452**, 1105–1111 (2015). DOI 10.1093/mnras/stv1336. 1505.06880.

21. Simcoe, R. A. *et al.* Extremely metal-poor gas at a redshift of 7. *Nat.* **492**, 79–82 (2012). DOI 10.1038/nature11612. 1212.0548.

22. Songaila, A. & Cowie, L. L. The Evolution of Lyman Limit Absorption Systems to Redshift Six. *Astrophys. J* **721**, 1448–1466 (2010). DOI 10.1088/0004-637X/721/2/1448. 1007.3262.

23. Zheng, Z.-Y. *et al.* First Results from the Lyman Alpha Galaxies in the Epoch of Reionization (LAGER) Survey: Cosmological Reionization at z $\sim$ 7. *Astrophys. J* **842**, L22 (2017). DOI 10.3847/2041-8213/aa794f. 1703.02985.

24. Gallerani, S., Fan, X., Maiolino, R. & Pacucci, F. Physical Properties of the First Quasars. *Public. Astron. Soc. Aust.* **34**, e022 (2017). DOI 10.1017/pasa.2017.14. 1702.06123.

25. Pâris, I. *et al.* The Sloan Digital Sky Survey Quasar Catalog: Twelfth data release. *Astron. Astrophys.* **597**, A79 (2017). DOI 10.1051/0004-6361/201527999. 1608.06483.

26. Fan, X. *et al.* Constraining the Evolution of the Ionizing Background and the Epoch of Reionization with z˜6 Quasars. II. A Sample of 19 Quasars. *Astron. J.* **132**, 117–136 (2006). DOI 10.1086/504836. arXiv:astro-ph/0512082.

27. Eilers, A.-C. *et al.* Implications of z$\sim$6 Quasar Proximity Zones for the Epoch of Reionization and Quasar Lifetimes. *Astrophys. J* **840**, 24 (2017). DOI 10.3847/1538-4357/aa6c60. 1703.02539.

28. Suzuki, N., Tytler, D., Kirkman, D., O'Meara, J. M. & Lubin, D. Predicting QSO Continua in the Lyα Forest. *Astrophys. J* **618**, 592–600 (2005). DOI 10.1086/426062. astro-ph/0306577.

29. Pâris, I. *et al.* A principal component analysis of quasar UV spectra at z ˜ 3. *Astron. Astrophys.* **530**, A50 (2011). DOI 10.1051/0004-6361/201016233. 1104.2024.

30. Alvarez, M. A. & Abel, T. Quasar HII regions during cosmic reionization. *Mon. Not. R. Astron. Soc.* **380**, L30–L34 (2007). DOI 10.1111/j.1745-3933.2007.00342.x. astro-ph/0703740.

31. Davies, F. B., Furlanetto, S. R. & McQuinn, M. Quasar ionization front Lyα emission in an inhomogeneous intergalactic medium. *Mon. Not. R. Astron. Soc.* **457**, 3006–3023 (2016). DOI 10.1093/mnras/stw055. 1409.0855.

32. Lukić, Z. *et al.* The Lyman α forest in optically thin hydrodynamical simulations. *Mon. Not. R. Astron. Soc.* **446**, 3697–3724 (2015). DOI 10.1093/mnras/stu2377. 1406.6361.

33. Mesinger, A., Furlanetto, S. & Cen, R. 21CMFAST: a fast, seminumerical simulation of the high-redshift 21-cm signal. *Mon. Not. R. Astron. Soc.* **411**, 955–972 (2011). DOI 10.1111/j.1365-2966.2010.17731.x. 1003.3878.

34. Drovandi, C. C., Pettitt, A. N. & Lee, A. Bayesian Indirect Inference Using a Parametric Auxiliary Model. *ArXiv e-prints* (2015). 1505.03372.

35. Bolton, J. S. *et al.* How neutral is the intergalactic medium surrounding the redshift z = 7.085 quasar ULAS J1120+0641? *Mon. Not. R. Astron. Soc.* **416**, L70–L74 (2011). DOI 10.1111/j.1745-3933.2011.01100.x. 1106.6089.

36. Foreman-Mackey, D., Hogg, D. W., Lang, D. & Goodman, J. emcee: The MCMC Hammer. *PASP* **125**, 306 (2013). DOI 10.1086/670067. 1202.3665.

37. Telfer, R. C., Zheng, W., Kriss, G. A. & Davidsen, A. F. The Rest-Frame Extreme-Ultraviolet Spectral Properties of Quasi-stellar Objects. *Astrophys. J* **565**, 773–785 (2002). DOI 10.1086/324689. astro-ph/0109531.

Acknowledgments: We thank D. Ossip for his support with the FIRE echellete observations and A. Stephens for his help preparing the GNIRS observations. This work is based on data collected with the Magellan Baade telescope, the Gemini North telescope (program GN-2017A-DD-4), the Large Binocular Telescope, and the IRAM/NOEMA interferometer. We are grateful for the support provided by the staff of these observatories. We acknowledge the use of the UKIDSS, *WISE*, and DECaLS surveys.

Author contributions: E.B., R.D., X.F., E.P.F., C.M., H.-W.R., D.S., B.P.V., F.W., F.W., and J.Y. discussed and planned the candidate selection, observing strategy, and analyzed the data. E.B. selected the quasar and with D.S. took and analyzed the discovery spectrum. R.S. provided the final FIRE data reduction. J.F.H. provided the final GNIRS data reduction. G.R. carried out the follow-up Fourstar observations for this quasar. D.K. reduced the follow-up Fourstar data. J.M.W., B.P.V., and F.W. contributed with the observations and analysis of the IRAM/NOEMA data. The Lyα damping wing analyses were carried out by E.B. (main manuscript, Model A), F.D. and J.F.H (Methods section, Model B) and R.S. and M.L.T. (Methods section, Model C). F.D. and J.F.H. did the PCA continuum modeling described in the Methods section. R.S. performed the analysis to find the characteristics of a single absorber that could cause the quasar's absorption profile. E.B. led the team and prepared the manuscript. All co-authors discussed the results and provided input to the paper and data analysis.

Author information: Reprints and permissions information is available at www.nature.com/reprints. The authors declare no competing financial interests. Correspondence and requests for materials should be addressed to ebanados@carnegiescience.edu.

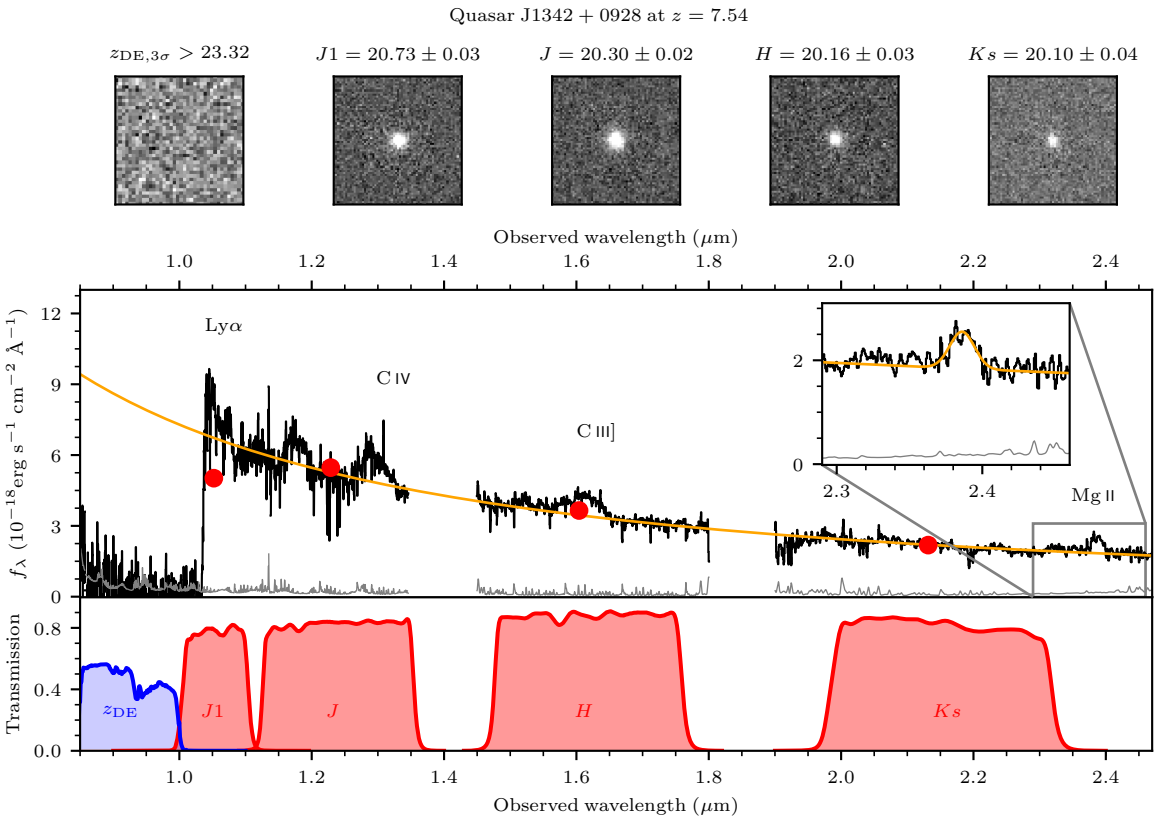

Figure 1. Photometry and combined Magellan/FIRE and Gemini/GNIRS near-infrared spectrum of the quasar J1342+0928 at $z = 7.54$. The FIRE data were taken on 11–12 March 2017 for a total integration time of 3.5 hr. We used the 0.6″ slit in the echellete mode, yielding a spectral resolution of $R \sim 6000$ over the range $0.8 - 2.3\,\mu$m. The GNIRS spectrum was obtained on 31 March 2017 and 03 April 2017 with a total exposure time of 4.7 hr. We used the 0.675″ slit in the cross-dispersion mode, yielding a spectral resolution of $R \sim 1800$ over the range $0.8 - 2.5\,\mu$m. The spectra are shown at the GNIRS resolution binned by a factor of two. The 1σ error is shown in gray and the orange line represents the best-fit power-law continuum emission with $f_\lambda \propto \lambda^{-1.58\pm0.02}$. Regions with low sky transparency between the J/H and H/Ks bands are not shown. The red circles show the follow-up photometry taken with the Magellan/Fourstar infrared camera. The inset shows a Gaussian fit to the Mg II line, from which we derive a black hole mass of $7.8 \times 10^8\,M_\odot$. The bottom panel shows the transmission of the Fourstar $J1$, J, H, Ks (red), and the DECam $z_{\rm DE}$ (blue) filters, while the top panel shows $10'' \times 10''$ postage stamps of the quasar in the same filters with their respective AB magnitudes.

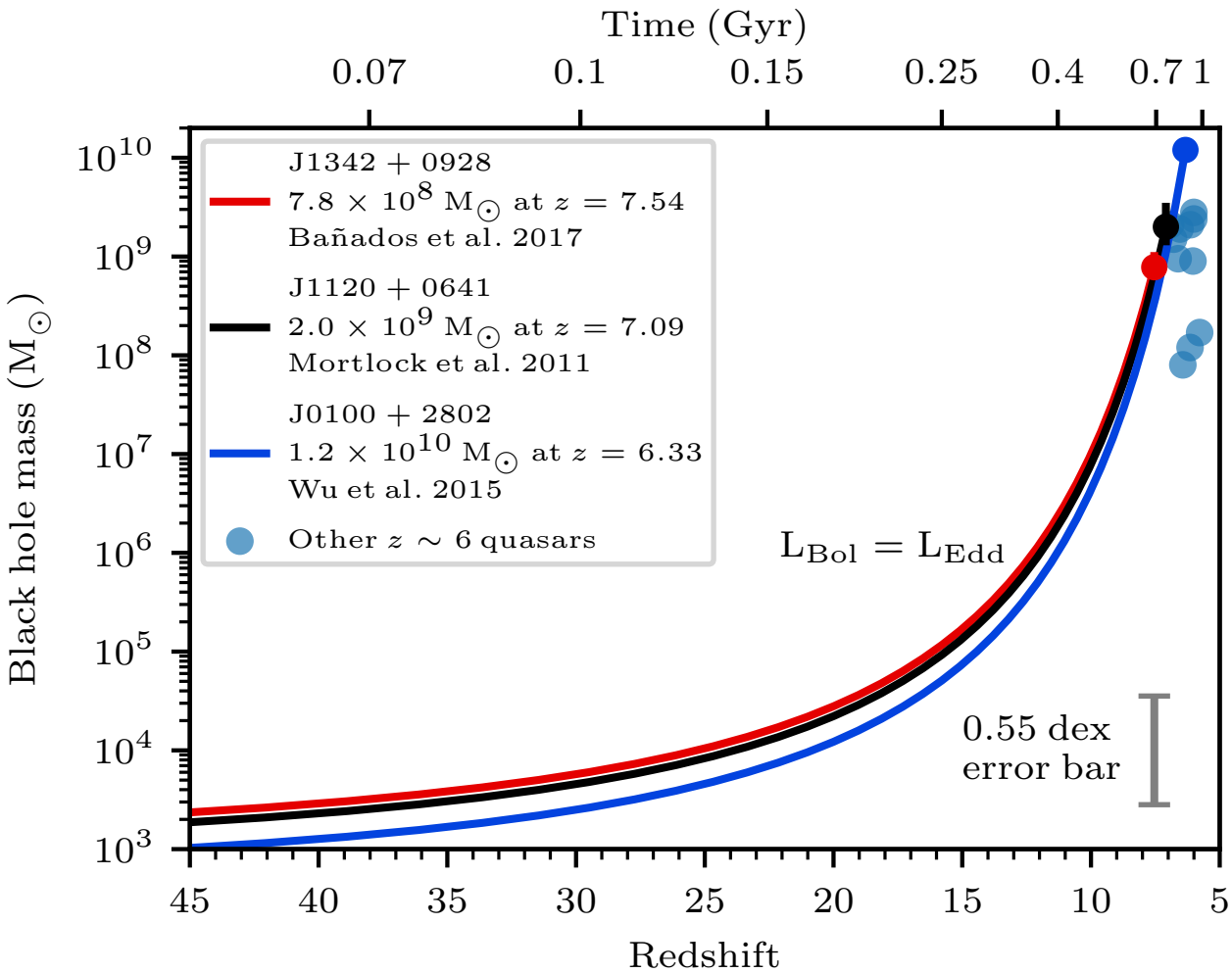

Figure 2. Black hole growth of three of the highest redshift and most massive quasars in the early universe, J1342+0928, J1120+0641[1], and J0100+2802[16]. The three curves are normalized to the observed black hole mass and redshift of these quasars (data points with statistical error bars). The black hole growth is modeled as $M_{\rm BH} = M_{\rm BH,seed} \times \exp(\text{time}/50\,\text{Myr})$, where we have assumed that the black holes are accreting at the Eddington limit ($L_{\rm Bol} = L_{\rm Edd}$) with a radiative efficiency of 10%. The circles show a compilation of black hole masses of $z \sim 6$ quasars[24]. The gray error bar at the bottom right represents dominant uncertainty due to systematics in the local scaling relation used to estimate the black hole mass of quasars at these redshifts[13]. Ignoring this systematic uncertainty and assuming that the local relations apply to these extremely distant and luminous quasars, black hole mass seeds more massive than $1000\,M_\odot$ by $z = 40$ are required to grow the observed supermassive black holes in all three cases.

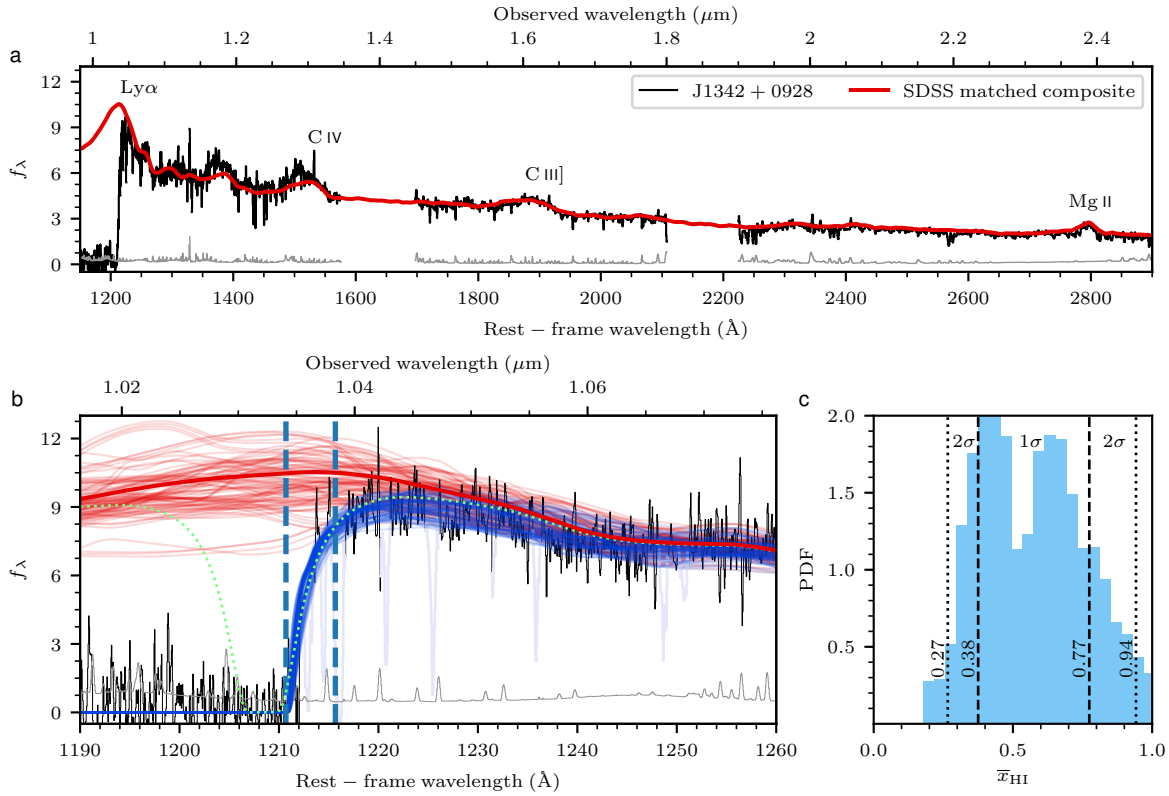

Figure 3. Continuum emission and Lyα damping wing modeling in the spectrum of J1342+0928 (in units of 10^{-18} erg s^{-1} cm^{-2} Å^{-1}). **a,** Same quasar spectrum shown in Figure. 1. The continuum model in red is constructed by averaging the SDSS DR12 quasars[25] not flagged as broad-absorption line quasars in the redshift interval $2.1 < z_{\rm Mg\,II} < 2.4$, and with a median S/N > 5 in the C IV region. The subsample was further refined considering only SDSS quasars with a C IV blueshift with respect to Mg II within 1000 km s^{-1} of that observed in J1342 + 0928 (6090 ± 275 km s^{-1}) and with rest-frame C IV equivalent widths consistent at the 3σ-level with the C IV equivalent width of J1342 + 0928 (EW = 11.3 ± 0.8 Å). This yielded 46 'analog' quasars. Their continua were individually fit by a slow-varying spline to remove strong absorption systems, noisy regions, and interpolate between high transmission peaks blueward of Lyα. We then normalized each spectrum at 1290 Å and averaged them. This composite spectrum is shown in red, and reproduces fairly well the spectral features of J1342 + 0928. Assuming the systemic redshift derived from [C II], the proximity zone of J1342 + 0928, which is defined[26,27] as the physical radius at which the transmission drops to 10%, is 1.3 Mpc. **b,** Zoom-in to the Lyα region showing a strong absorption profile that can be modeled as a Lyα damping wing caused by a significantly neutral IGM. The black and gray curves are the FIRE spectrum and 1σ error binned by a factor of two. The pale gray lines show regions masked out due to intervening absorption systems. The thick red line is the SDSS matched composite spectrum (see panel a) while the thin red lines are used as intrinsic emission models (100 out of 3000 shown). To take into account the error in the *prediction* for any given quasar, these models consist of bootstrapped mean composite spectra plus a relative error vector (SDSS quasar - mean)/mean randomly chosen among the 46 possible error vectors. The blue lines represent the expected IGM damping wing following the prescription of Miralda-Escudé (1998)[18] assuming a fully ionized proximity zone (region between the vertical dashed lines), a constant neutral fraction $\bar{x}_{\rm HI}$ between the end of the quasar's proximity zone and $z = 7.0$, and a fully ionized IGM at $z < 7$. The exact choice of the transition redshift does not significantly affect the results. The green dotted line is the absorption that would be caused by a single absorber with $N_{\rm HI} = 10^{20.5}$ cm^{-2} at $z = 7.49$. **c,** The derived $\bar{x}_{\rm HI}$ probability density function (PDF), with a preferred value of $\bar{x}_{\rm HI} = 0.56^{+0.21}_{-0.18}$. In the Methods section we present one additional model of the quasar's intrinsic emission and two additional models of the IGM damping wing. All our analyses require a significantly neutral IGM to reproduce the damping wing profile in the spectrum of J1342 + 0928 (see Extended Data Table 2).

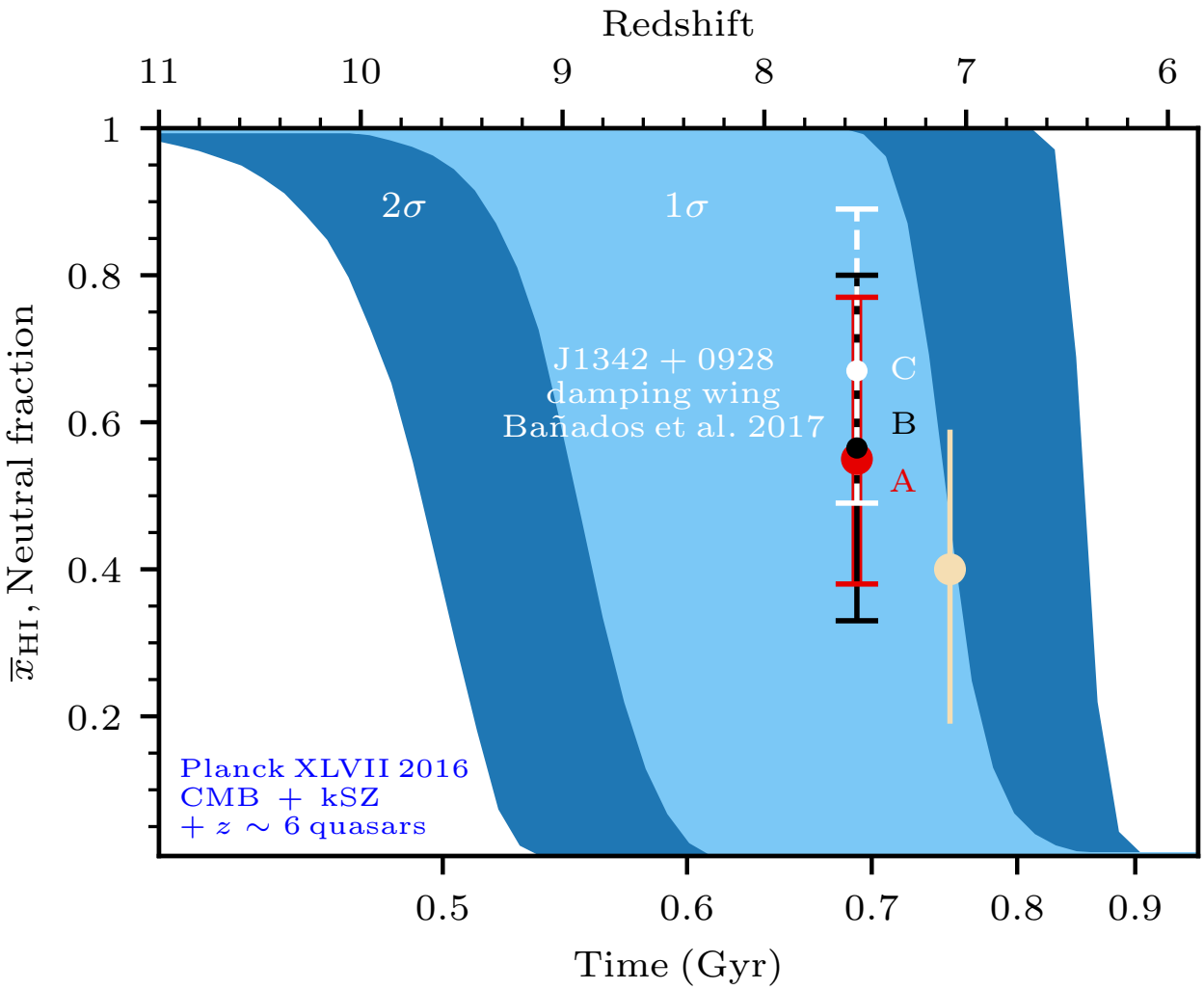

Figure 4. Constraints on the history of reionization in terms of hydrogen neutral fraction vs. cosmic time from the Big Bang in gigayears (redshift on the top axis). The contours show the 1σ and 2σ constraints from the optical depth to the Cosmic Microwave Background (CMB), the kinetic Sunyaev-Zeldovich (kSZ) effect, and $z \sim 6$ quasars compiled by the Planck collaboration[12] (see their Figure 17 and references therein). The data points represent the 1σ constraints from the damping wing analyses of J1120+0641 at $z = 7.09$[19] ($\overline{x}_{\rm HI} = 0.40^{+0.21}_{-0.19}$) and J1342 + 0928 at $z = 7.54$. The red error bar represents the analysis presented in Figure 3, while the black and white measurements are the most conservative constraints (i.e., lower neutral fraction) from the two additional models (B and C) of the Lyα damping wing of J1342 + 0928 presented in the Methods section (see Extended Data Table 2). All our analyses consistently find a large fraction of neutral hydrogen surrounding J1342 + 0928. The uncertainties in the IGM damping wing analyses do not include cosmic variance, i.e., we are constraining one line-of-sight per quasar. In order to better comprehend the global history of reionization would require additional measurements at similar redshifts along more lines of sight. We note that the quasar IGM damping wing constraints shown in this figure have used a range of methods to perform the analysis and thus have different systematics.

Methods

Lyα damping wing modeling

As discussed in the main manuscript, in order to calculate the intergalactic medium (IGM) neutral fraction ($\bar{x}_{\rm HI}$), one must first estimate the quasar's intrinsic emission. After that, a model is fit that reproduces the observed damping wing in the Lyα region. In the main manuscript, we show that the data strongly suggests that the IGM in the surrounding of the quasar J1342 + 0928 at $z = 7.54$ is significantly neutral: $\bar{x}_{\rm HI} = 0.56^{+0.21}_{-0.18}$ (see Figure 3). Recovering the intrinsic continuum of J1342 + 0928 is particularly challenging because of its extreme emission line blueshifts, which are not well represented in matched composites at lower redshifts. Specifically, in the analysis presented in the manuscript we found only 46 lower-redshift quasars with similar C IV blueshifts and equivalent widths. Furthermore, in the main manuscript we have modeled the IGM Gunn-Peterson damping wing following a prescription17 that assumes a homogeneous neutral IGM between the quasar's proximity zone and an arbitrary redshift, which we set to $z_{\rm END} = 7.0$ and considers the universe to be completely ionized below that redshift. We remark that given that the damping wing is produced by the IGM in the environment of the quasar, the results are insensitive to the exact value of $z_{\rm END}$. For example, the results change only by less than 1% even in the extreme case of $z_{\rm END} = 6.0$. Hereafter, we refer to the IGM model presented in the main manuscript as Model A.

Here we reanalyze the data presenting an additional model of the quasar's intrinsic emission using a principal component analysis (PCA) decomposition. Furthermore, we introduce two completely independent methods to model the IGM damping wing using the quasar's intrinsic emission obtained in the main manuscript (SDSS matched composite, hereafter continuum 1) and the PCA-model (hereafter continuum 2; described in more detail below) as inputs. In this way, we test how sensitive our conclusions are to different assumptions and systematics in the analysis.

Quasar's intrinsic emission – PCA model

In this model, we predict the intrinsic quasar continuum in the Lyα region ($\lambda_{\rm rest} < 1260$ Å) based on the rest of the spectrum using a PCA analysis trained on 12764 quasar spectra from the SDSS/BOSS DR12 quasar catalog[25]. Quasars in the training set were chosen to have S/N > 7 at $\lambda_{\rm rest} < 1285$ Å and to lie at redshifts $2.1 < z < 2.5$ such that the BOSS spectral range comfortably covered the Lyα region (down to $\lambda_{\rm rest} = 1190$ Å) and the Mg II region up to $\lambda_{\rm rest} \sim 2800$ Å, similar to the rest-frame spectral coverage of J1342 + 0928. We constructed red-side and blue-side PCA basis spectra from the training set after applying automated spline fits to recover the unabsorbed continuum. For each quasar in the training set, we simultaneously fit for the PCA coefficients and a template redshift, placing each quasar into a common "PCA redshift frame" independent of (but largely similar to) their catalog redshifts. We used these fits to define the matrix projection from red-side to blue-side PCA coefficients as in Suzuki et al. (2005)[28] and Pâris et al. (2011)[29]. We then fit the red-side PCA coefficients of J1342+0928 in the same way as the training set. To estimate the bias and uncertainty of the continuum fit for quasars similar to J1342+0928, we measured the relative continuum error for the 1% of quasars in the training set with the most similar red-side PCA coefficients. The relative uncertainty in the Lyα region for this subset was found to be ~7%.

In Figure E1 we compare the quasar's intrinsic Lyα emission reconstructed by both the PCA and SDSS-matching analyses. The PCA continuum predicts a slightly stronger emission in the Lyα region but in both cases the emission is significantly weaker than for an average low-redshift SDSS quasar.

IGM damping wing

Using continuum 2 (PCA) as input for Model A, we require a virtually completely neutral universe, $\bar{x}_{\rm HI} \sim 1$, to model the Lyα damping wing in the spectrum of J1342+0928. This is driven by the higher intrinsic flux in the Lyα region of continuum 2. We would obtain an even more dramatic result if we naively used an average SDSS quasar as input, which would have a much stronger Lyα emission line (Figure E1). Altogether, this seems to reinforce our findings that the universe is significantly neutral at $z \sim 7.5$. To assess whether this result is dependent on the method used to reproduce the IGM damping wing, we here introduce two more elaborated methods (hereafter Models B and C).

Model B

In this model, we place the quasar within simulated massive dark matter halos at $z = 7.5$, which in turn populate large-scale overdensities already ionized by galaxies before the quasar turns on[30]. The damping wing strength is then sensitive to the distance to the nearest neutral patch set by the morphology of reionization, as well as the output of ionizing photons from J1342+0928. Small proximity zones can result either from a high $\bar{x}_{\rm HI}$ in the surrounding IGM, or from a short active lifetime of the central quasar[27]. We modeled the residual H I absorption inside the quasar proximity zone and the damping wing profile from the neutral IGM by simulating the radiative transfer of ionizing photons through the IGM[31] from the locations of massive dark matter halos using realistic distribution of densities from a large-volume hydrodynamical simulation[32]. The inside-out morphology of reionization as a function of $\bar{x}_{\rm HI}$ was computed from independent large-volume semi-numerical simulations of patchy reionization using a modified version of the 21cmFAST code[33].

The hydrogen neutral fraction $\bar{x}_{\rm HI}$ and quasar lifetime t_Q were then jointly constrained via a Bayesian approach using pseudo-likelihood in the spirit of indirect inference methods (e.g., Drovandi et al. 2015[34]). We define our pseudo-likelihood as the product of independent flux PDFs evaluated in 500 km s^{-1} spectral bins, and treat the set of maximum pseudo-likelihood parameter values (i.e., $\bar{x}_{\rm HI}$ and t_Q) as a summary statistic.

We applied Model B to the quasar continuum obtained from the PCA method described above, employing millions of forward-modeled mock spectra, including a self-consistent treatment of the highly covariant continuum (determined from our PCA training set described above), to compute the posterior PDF. Marginalizing over quasar lifetimes with a log-uniform prior in the range $10^5 < t_Q < 10^8$ years, the central 68% (95%) credible interval for $\bar{x}_{\rm HI}$ is $0.45-0.87$ ($0.22-0.98$). We show a representation of Model B using the PCA-model intrinsic emission and its marginalized posterior PDF of $\bar{x}_{\rm HI}$ in Figure E2.

If we apply Model B using the SDSS matched intrinsic emission models as input, the central 68% (95%) credible interval for $\bar{x}_{\rm HI}$ is $0.33-0.80$ ($0.11-0.96$) and we show the posterior PDF of $\bar{x}_{\rm HI}$ in Figure E3a.

Model C

In this model, the IGM absorption profile is modeled based on the methods outlined in Bolton et al. (2011)[35]. After the quasar turns on, it evacuates an expanding ionized region (the proximity zone) within the surrounding IGM. Its absorption profile is then specified by four parameters: (1) the quasar's ionizing luminosity (constrained by photometry), (2) the proximity zone size (related to the quasar age), (3) the mean density of the surrounding medium, and (4) $\bar{x}_{\rm HI}$ outside the proximity zone. We use an affine-invariant Markov Chain Monte Carlo (MCMC) solver[36] to fit these four parameters. The quasar's ionizing luminosity is estimated using the power law indices from Telfer et al. (2002)[37] and the quasar magnitudes from this work. We impose a Gaussian prior with a width determined from the power law index errors from Telfer et al. (2002)[37], while the remaining parameters are all given flat priors.

Before fitting our model, we apply an automated clipping procedure to remove spectral absorption features. We divide the normalized spectrum into bins of size 2.5 Å in the rest-frame, and interpolate a B-spline through the mean flux in each bin. Any pixels with flux values $> 3\sigma$ below or $> 7\sigma$ above the interpolated values are masked. This procedure is repeated until convergence is achieved. Then, we ran two MCMC realizations, one for each mean quasar continuum created above (1 and 2, see Figure E1). For each continuum model, we ran 100 chains of 2000 steps each, and use the final 200 steps to construct the posteriors (the burn-in occurs within the first $\sim$250 steps).

For continuum 1, the central 68% (95%) credible interval for $\bar{x}_{\rm HI}$ is $0.49-0.89$ ($0.31-0.99$) and its posterior PDF is shown in Figure E3b. On the other hand, Model C requires a neutral universe ($\bar{x}_{\rm HI} \sim 1$) if continuum 2 is used as input, in line with the result obtained using Model A.

Final remarks

In Extended Data Table 2 we summarize the constraints on the neutral fraction obtained by all IGM modeling methods used in this article with the two different models of the quasar intrinsic emission. In all cases we recover a large IGM neutral fraction in agreement with the analysis presented in the main manuscript. In Figure 4, we show a comparison between these three models. To be conservative, we show the constraints obtained by using continuum 1 as input as it predicts a weaker emission around the Lyα line than continuum 2 (Figure E1) and thus lower neutral fractions are needed to explain the absorption profile in J1342+0928 (Extended Data Table 2). The most conservative of the analysis is Model B, which prefers a $\bar{x}_{\rm HI} > 0.11$ IGM at the 2σ level (see Figure E3a), being one of strongest constraints yet in the history of reionization.

Data availability: The datasets generated and analyzed during this study are available from the corresponding author on reasonable request.

Code availability: We have opted not to make available the codes presented in the Method Section to model the IGM damping wing because they will be described in more detail and made available in forthcoming papers (F. Davies et al. [Model B] and M.L Turner et al. [Model C]).

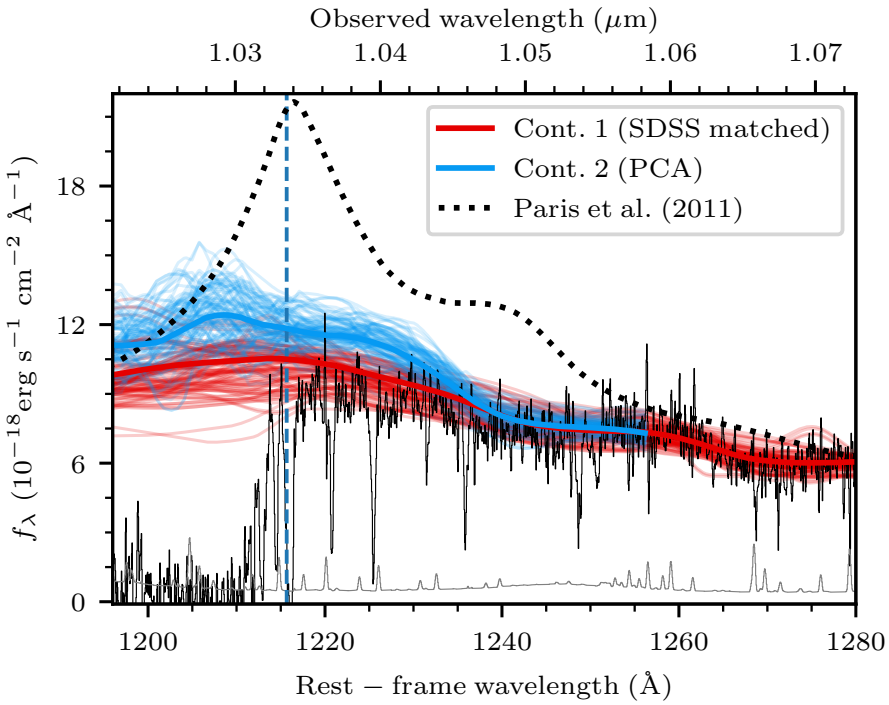

Figure E1. J1342+0928's intrinsic emission modeling. The red lines represent the continuum used in the main manuscript constructed by averaging SDSS DR12 quasars with similar C IV properties (EWs and blueshifts) of that observed in J1342 + 0928 (see Figure 3). The light blue lines are 100 random draws of PCA-reconstructed intrinsic emission as described in the Methods section. In both cases, the mean intrinsic spectrum is shown as a thick line. The vertical dashed line shows the Lyα wavelength. The PCA-reconstructed spectrum has a stronger emission around the Lyα line than the SDSS matched reconstructed emission. The dotted line is the mean SDSS quasar from Pâris et al. (2011)[29], which has a much stronger Lyα line than that of any of our continuum models of J1342 + 0928.

Table E1. Survey photometry of the quasar J1342+0928 at z = 7.54.

Survey	AB magnitudes	
DECaLS	$z_{\mathrm{DE},3\sigma} > 23.32$	
UKIDSS	$Y = 21.47 \pm 0.19$	$J = 20.75 \pm 0.11$
	$H = 20.02 \pm 0.02$	$K = 20.03 \pm 0.12$
WISE	$W1 = 20.17 \pm 0.15$	$W2 = 20.11 \pm 0.29$

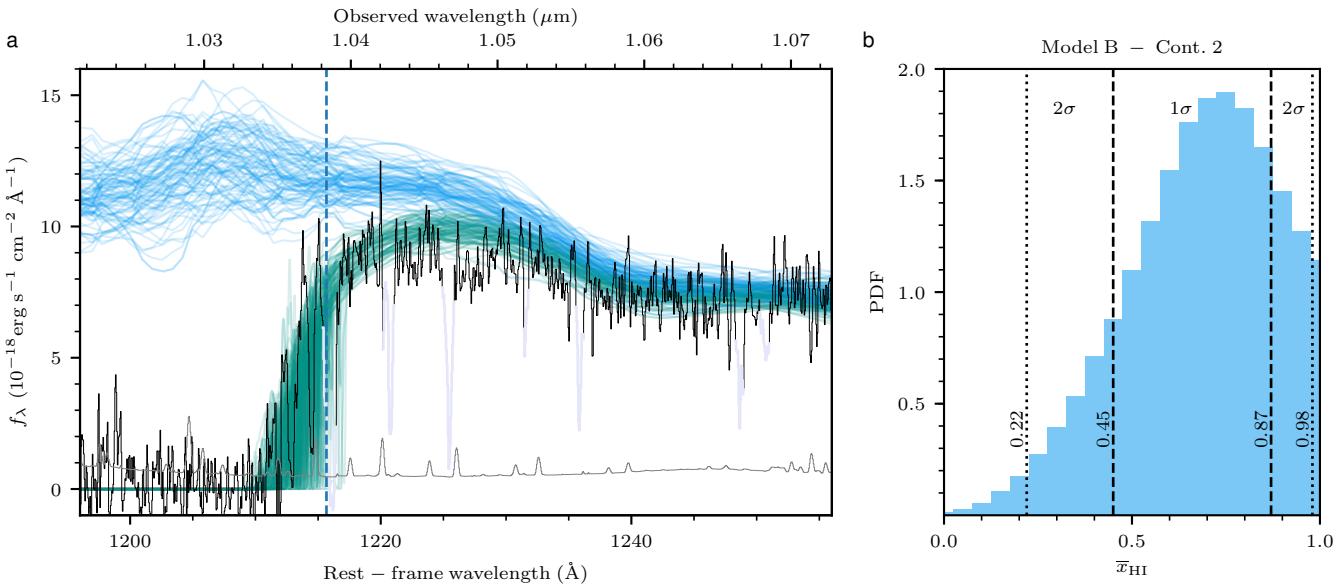

Figure E2. Model B IGM damping wing analysis with PCA continuum. a, Same as Figure 3b but this time showing 100 realizations of the PCA-predicted intrinsic emission (light blue) and IGM damping wing (green) model draws from the posterior PDF of Model B (see text in Methods section for details). Model B masks absorption systems only redward of the Lyα line (pale gray) as this model takes into account the internal absorption in the proximity zone, which explains the larger scatter blueward of Lyα (dashed vertical line). **b,** The marginalized posterior PDF of $\bar{x}_{\rm HI}$. The 50th percentile is $\bar{x}_{\rm HI} = 0.68$ while the 16th – 84th (2.5th – 97.5th) percentile interval is $0.45 - 0.87$ ($0.22 - 0.98$).

Table E2. Summary of the constraints on the neutral fraction $\bar{x}_{\rm HI}$ in the surroundings of the quasar J1342+0928. $\bar{x}_{\rm HI}$ constraints from the modeling of the quasar's Lyα damping wing with three different IGM models and two different intrinsic emission modeling. The central 68% (95%) credible intervals are reported, except when a completely neutral IGM is always the preferred solution $\bar{x}_{\rm HI} \sim 1$.

Continuum \ IGM Model	A – 68% (95%)	B – 68% (95%)	C – 68% (95%)
1 (SDSS-matched)	$0.38 - 0.77$ ($0.27 - 0.94$)	$0.33 - 0.80$ ($0.11 - 0.96$)	$0.49 - 0.89$ ($0.36 - 0.98$)
2 (PCA)	~ 1	$0.45 - 0.87$ ($0.22 - 0.98$)	~ 1

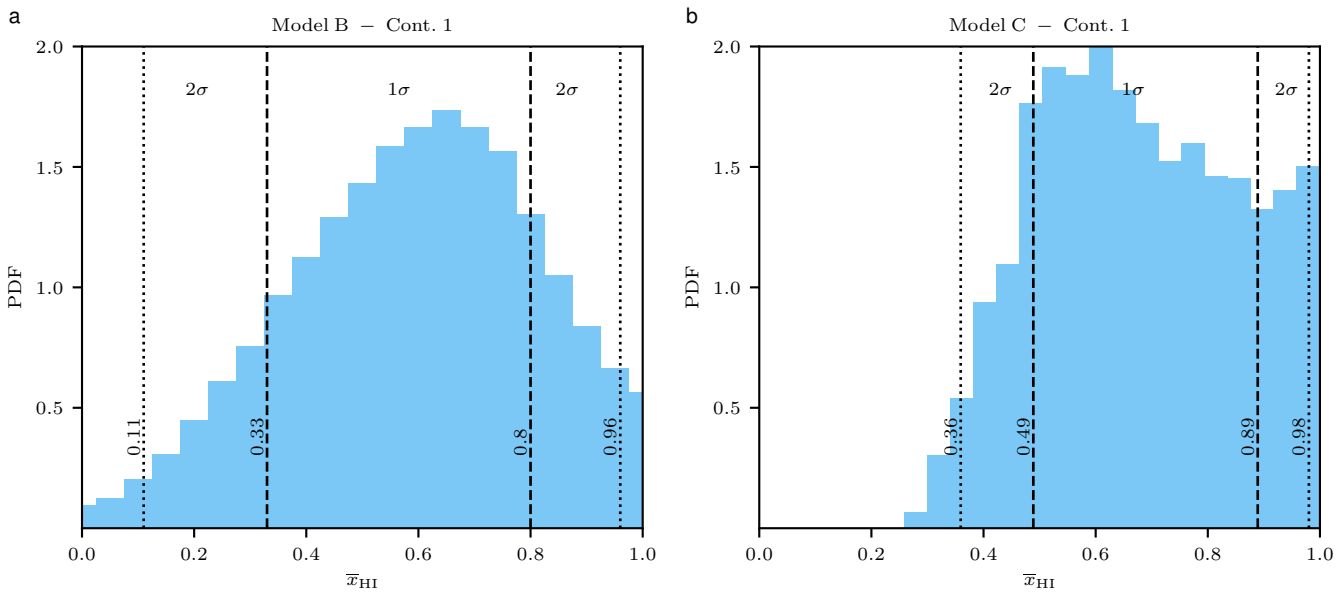

Figure E3. The marginalized posterior PDF of $\overline{x}_{\rm HI}$ using continuum 1 (SDSS-matched) as input for IGM Model B (panel a) and Model C (panel b). Model B applied to continuum 1 yields the most conservative distribution of our analyses. Even in this case, a significantly neutral universe with $\overline{x}_{\rm HI} > 0.11$ at the 2σ level is preferred.